

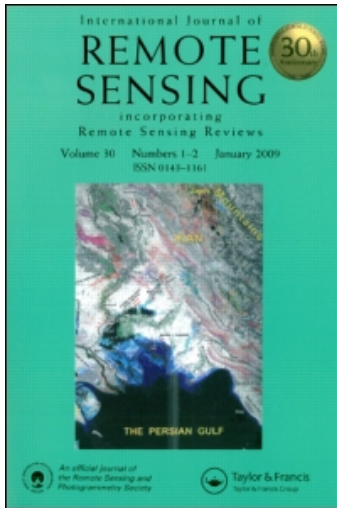
This article was downloaded by: [Ingenta Content Distribution - Routledge]

On: 19 March 2010

Access details: Access Details: [subscription number 791963552]

Publisher Taylor & Francis

Informa Ltd Registered in England and Wales Registered Number: 1072954 Registered office: Mortimer House, 37-41 Mortimer Street, London W1T 3JH, UK



International Journal of Remote Sensing

Publication details, including instructions for authors and subscription information:

<http://www.informaworld.com/smpp/title~content=t713722504>

Tsunami observations by coastal ocean radar

M. L. Heron ^a; A. Prytz ^a; S. F. Heron ^b; T. Helzel ^c; T. Schlick ^d; D. J. M. Greenslade ^e; E. Schulz ^e; W. J. Skirving ^b

^a AIMS@JCU and Marine Geophysical Laboratory, James Cook University, Townsville, Australia ^b NOAA/NESDIS Coral Reef Watch, Silver Spring, MD, USA ^c Helzel Messtechnik GmbH, Kaltenkirchen, Germany ^d University of Hamburg, Germany ^e Bureau of Meteorology Research Centre, Melbourne, Australia

To cite this Article Heron, M. L., Prytz, A., Heron, S. F., Helzel, T., Schlick, T., Greenslade, D. J. M., Schulz, E. and Skirving, W. J.(2008) 'Tsunami observations by coastal ocean radar', International Journal of Remote Sensing, 29: 21, 6347 – 6359

To link to this Article: DOI: 10.1080/01431160802175371

URL: <http://dx.doi.org/10.1080/01431160802175371>

PLEASE SCROLL DOWN FOR ARTICLE

Full terms and conditions of use: <http://www.informaworld.com/terms-and-conditions-of-access.pdf>

This article may be used for research, teaching and private study purposes. Any substantial or systematic reproduction, re-distribution, re-selling, loan or sub-licensing, systematic supply or distribution in any form to anyone is expressly forbidden.

The publisher does not give any warranty express or implied or make any representation that the contents will be complete or accurate or up to date. The accuracy of any instructions, formulae and drug doses should be independently verified with primary sources. The publisher shall not be liable for any loss, actions, claims, proceedings, demand or costs or damages whatsoever or howsoever caused arising directly or indirectly in connection with or arising out of the use of this material.

Tsunami observations by coastal ocean radar

M. L. HERON*†, A. PRYTZ†, S. F. HERON‡, T. HELZEL§, T. SCHLICK¶,
D. J. M. GREENSLADE#, E. SCHULZ# and W. J. SKIRVING‡

†AIMS@JCU and Marine Geophysical Laboratory, James Cook University,
Townsville, Australia

‡NOAA/NESDIS Coral Reef Watch, Silver Spring, MD, USA

§Helzel Messtechnik GmbH, Kaltenkirchen, Germany

¶University of Hamburg, Germany

#Bureau of Meteorology Research Centre, Melbourne, Australia

(Received 24 April 2007; in final form 31 March 2008)

When tsunami waves propagate across the open ocean, they are steered by the Coriolis effect and refraction due to gentle gradients in the bathymetry on scales longer than the wavelength. When the wave encounters steep gradients at the edges of continental shelves and at the coast, the wave becomes nonlinear and conservation of momentum produces squirts of surface current at the head of submerged canyons and in coastal bays. High frequency (HF) coastal ocean radar is well conditioned to observe the surface current bursts at the edge of the continental shelf and give a warning of 40 minutes to 2 hours when the shelf is 50 to 200 km wide. The period of tsunami waves is invariant over changes in bathymetry and is in the range 2 to 30 minutes. Wavelengths for tsunamis (in 500 to 3000 m depth) are in the range 8.5 to over 200 km, and on a shelf where the depth is about 50 m (as in the Great Barrier Reef (GBR)) the wavelengths are in the range 2.5 to 30 km. In the use of HF radar technology, there is a trade-off between the precision of surface current speed measurements and time resolution. It is shown that the phased array HF ocean surface radar being deployed in the GBR and operating in a routine way for mapping surface currents, can resolve surface current squirts from tsunamis in the wave period range 20 to 30 minutes and in the wavelength range greater than about 6 km. An advantage in signal-to-noise ratio can be obtained from the prior knowledge of the spatial pattern of the squirts at the edge of the continental shelf, and it is estimated that, with this analysis, the time resolution of the GBR radar may be reduced to about 2.5 minutes, which corresponds to a capability to detect tsunamis at the shelf edge in the period range 5 to 30 minutes. It is estimated that the lower limit of squirt velocity detection at the shelf edge would correspond to a tsunami with water elevation of about 2.5 cm in the open ocean. This means that the GBR HF radar is well conditioned for use as a monitor of small, as well as larger, tsunamis and has the potential to contribute to the understanding of tsunami genesis research.

*Corresponding author. Email: mal.heron@jcu.edu.au

1. Introduction

1.1 Tsunami characteristics

Tsunamis are long wavelength, long period, ocean gravity waves that are normally produced by earthquakes or underwater slumps. The wave period of tsunamis depends upon the scale size of the bathymetric event and water depth. Historical records of impacts on the shore indicate that the tsunami wave period (the so-called tsunami window) is in the range 2 to 30 minutes (Bryant 2001). There is great variability in the relationship between earthquake intensity and tsunami generation; some marine earthquakes do not produce tsunamis and some tsunamis occur with quite small seismic activity. The bigger tsunamis are typically due to greater vertical motion in the rupture. Once the pulse of elevated water is produced, it can travel large distances with little attenuation and some dispersion. The amplitude of the tsunami waves in the open ocean is generally less than about 0.5 m. This is amplified at the shore and can produce run-up of over 100 m (Bryant 2001).

The Aceh tsunami on 26 December 2004 produced wave height at beaches across the Indian Ocean of the order of 10 m and the open ocean elevation was 0.5 m, as measured by the JASON-1 altimeter (Gower 2005, Smith *et al.* 2005) in the Indian Ocean some 2 hours after the earthquake in the Sumatra-Andaman Islands.

If we assume a tsunami amplitude of 20 cm in water of 10 m depth, then the simple shoaling relation, given by Kinsman (1965) as:

$$\frac{h_s}{h_d} = \left(\frac{H_d}{H_s} \right)^{1/4},$$

where h_s is the wave amplitude in water of depth H_s and h_d is the wave amplitude in water of depth H_d , may be used to find that the equivalent wave amplitude in 5 km depth is about 4 cm. While this is a simple linear relation, it gives an indication of the required resolution of a tsunami-observing instrument.

1.2 HF radar characteristics

High frequency (HF) ocean surface radar obtains high-energy echoes from Bragg waves on the ocean surface that have wavelengths equal to half the radar wavelength and that are propagating radially towards and away from the radar site. These are the first-order echoes, which are normally more than 10 db stronger than other echoes. The radial resolution scale for radars is inversely proportional to the bandwidth of the transmitted signal. For HF radars, this is typically 50 kHz and is controlled by international agreements on the use of the radio spectrum. Some systems are working with bandwidths up to 150 kHz. The radar being installed on the Great Barrier Reef (GBR) in Australia has a bandwidth of 33 kHz, which corresponds to a radial range resolution of 4.5 km, and an operating frequency of 8.348 MHz. The azimuthal resolution is controlled by the width of the lobe for beam-forming radars and by the accuracy of amplitude or phase measurements for direction-finding radars.

A typical radar spectrum is shown in figure 1. The offset of the Bragg peaks from the reference (which is the transmitter frequency) is due to Doppler shift. This is predominantly caused by the phase velocity of the Bragg waves (whose frequency offset is indicated by the vertical dashed lines to the left of peaks A and B in figure 1), but also caused by radial surface current (indicated by df in figure 1).

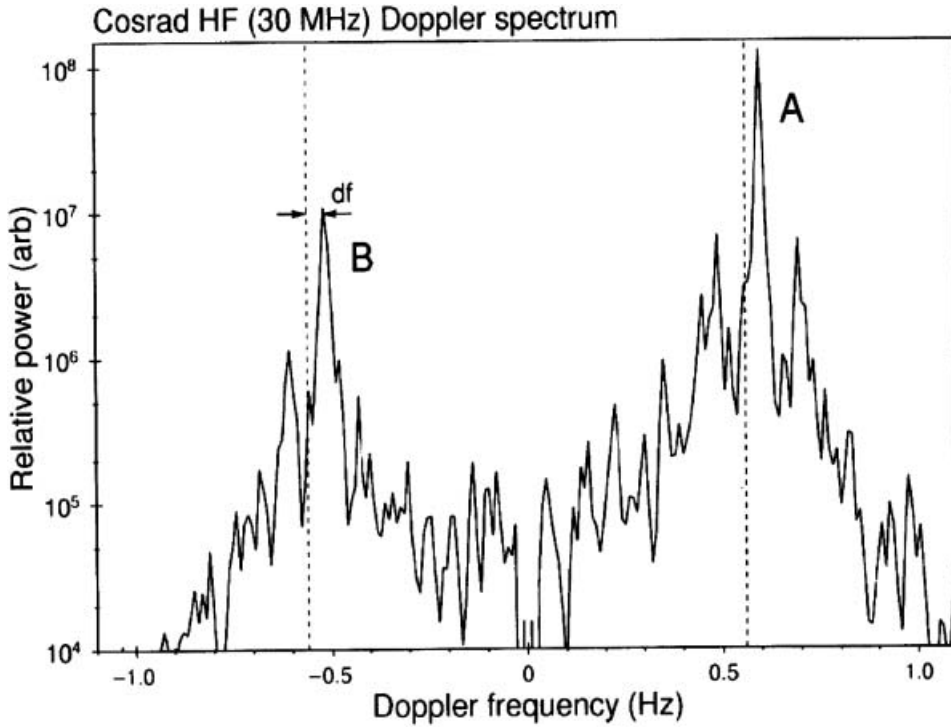


Figure 1. Typical spectrum for a phased array ocean surface radar. The peaks labelled A and B are the first-order Bragg scatter. The sideband peaks on each side of the Bragg lines are produced by wind waves.

Spectra from the GBR radar system have Bragg peaks at 0.295 Hz from the reference frequency, which is set to zero in figure 1. The question arises here about the differentiation between swell (which shows up as sidebands on the spectrum) and tides (which are effectively very long waves). We step around tsunamis here because they fall in between the two extremes and we will discuss them later. Tides have return periods much greater than the time it takes to observe the time series (which is the basis of the spectrum shown in figure 1), and the pixel size for the radar is much smaller than the length scale of the tidal cycles. Therefore, the tidal currents are resolved in time and space by the HF radars. Swell has wave periods much shorter than the duration of the time series, and the wavelength of swell is less than the pixel size for the radar. Therefore, swell is not resolved by successive time series samples. When swell is present, it appears as sidebands on the Bragg lines and separated from them by a frequency equal to the frequency of the swell; in this record, the swell lines are barely significant compared with fluctuations in the spectrum. In this paper, we investigate the time and space scales for tsunamis.

2. Tsunami period and wavelength

Tsunamis are shallow water gravity waves and we can use linear wave theory at least while the waves are in open water with gentle gradients in the bathymetry. The expression for wave celerity, c , for gravity waves is (Kinsman 1965):

$$c^2 = \frac{g}{k} \tanh(kH), \tag{1}$$

where k is the wave number, g is the gravitational acceleration and H is the water depth. In shallow water, a good approximation is:

$$c = \sqrt{gH}, \quad (2)$$

which is illustrated in figure 2 by a family of curves with H varying from 500 to 3000 m. The flat sections for wave periods above about 300 s confirm the applicability of equation (2), while, for smaller wave periods, equation (1) becomes more appropriate. One important indication from figure 2 is that for a pulse of water elevation at the source, the subsequent propagation will be subject to some dispersion for the higher frequency components (wave periods less than about 300 s), which means that for distant sources the first ocean waves will have periods longer than about 300 s.

3. Tsunami propagation

In open water, with gentle gradients in bathymetry, the wave direction is controlled by refraction and Coriolis rotation off great circle paths. The refractive steering of gravity waves is illustrated in figure 3(a), where a stylised shore line is shown in bold and accompanying bathymetry contours are also shown. Swell waves approaching the coast will be refracted by the gradients in bathymetry as shown, which tend to produce focusing by submerged ridges with defocusing in the bays. This is different

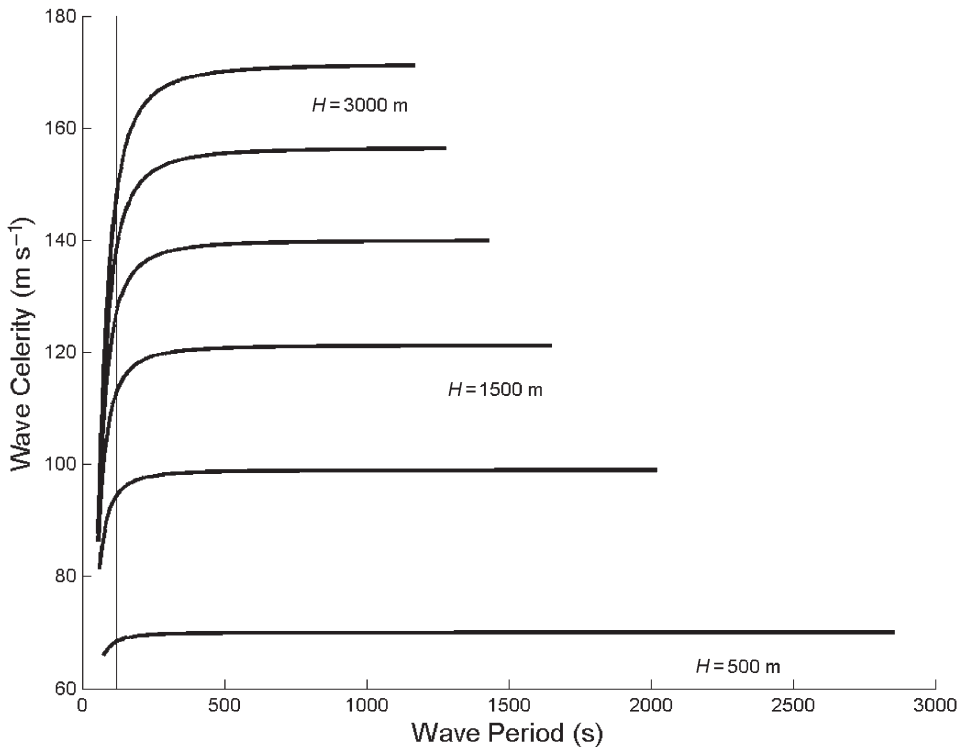


Figure 2. Properties of gravity waves derived from equation (1) for tsunami conditions. Celerity versus wave period shows the transition from dispersive conditions at short wave periods to no dispersion at long periods. The vertical marker at 120 s marks the shortest tsunami period (Bryant 2001). Water depth, H , is taken in 500 m intervals.

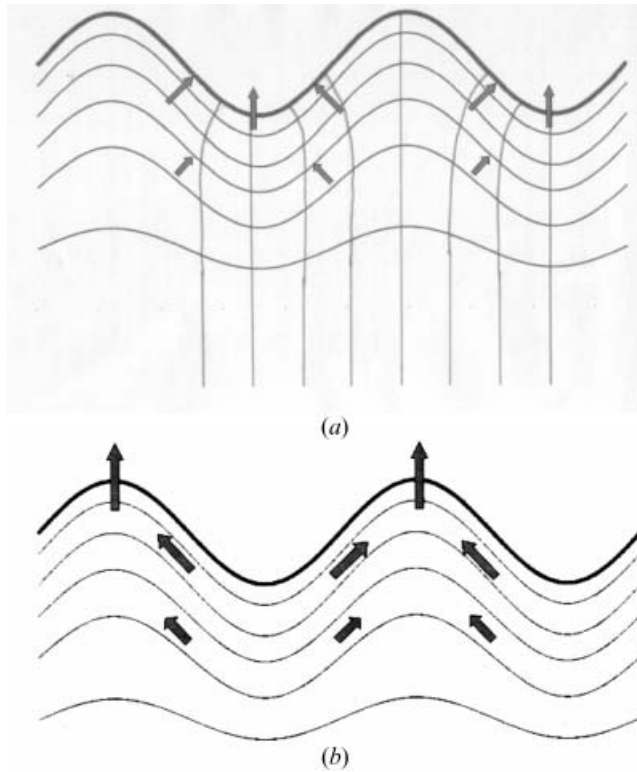


Figure 3. A stylised shore line (bold) at the top and offshore bathymetry contours: (a) refract swell energy and wind waves (entering the diagram along ray paths from the bottom) onto the headlands and away from the bays and (b) direct the momentum in a tsunami along the bathymetry contours to give the most intense effects in the bays.

from the observations of tsunami waves at the coast, which are more intense in the bays with run-up into the valleys. The apparent paradox where swell is enhanced at headlands and tsunamis are enhanced in the submarine canyons and into the bays is resolved by considering nonlinearities and spatial scales.

For tsunamis, nonlinear effects arise from the conservation of momentum in the water column, which tends to drive water parallel to the depth contours to produce enhancement of surface elevation at the head of submerged canyons, which in turn produces the greatest effect at the coast in bays and estuaries rather than at headlands. If the bathymetry changes significantly within one wavelength, then momentum effects dominate over refraction. In the open ocean (500 to 3000 m depth), wavelengths for tsunamis are in the range 8.5 to over 200 km, and because bathymetric gradients are gentle, we may assume that bathymetric steering in the open ocean is controlled by refraction. As a tsunami propagates across a basin it will normally be refracted so that it exits the basin orthogonally to the large-scale bathymetric contours. Near the coast, however, where the scale of the spatial features is less than the wavelength, refraction does not work because the wave is changing (by nonlinear effects) within the space of a wavelength. The water elevation (and run-up) is controlled by momentum transfer as the water becomes shallower.

Refractive steering is easy to calculate and was used for the ray paths shown in figure 3(a) for typical ocean swell. Figure 3(a) shows focusing (aggregation of ray

paths) at the headland with energy being steered away from the bay areas. For tsunami wavelengths where the spatial scale of the waves exceeds that of the coastal features, water is transferred along the bathymetry contours as the wave moves towards the coast, and the focusing is steered away from the headlands and into the bays as illustrated in figure 3(b). The momentum transfer is a result of nonlinear processes and is better modelled by numerical calculations than by an analytic wave propagation approach. An example of such a model is shown in figure 4, where the surface currents at the edge of the continental shelf near the Seychelles are shown for the first wave of the 26 December 2004 tsunami, which originated near Aceh, Indonesia. The relevant bathymetry is shown in figure 4(a). It can be seen that the higher current surges are produced at the heads of submerged canyons, while the submerged ridges experience smaller surges.

4. Time and space scales

4.1 Space scales for radar observation

The spatial resolution of HF radars in the radial dimension depends on the bandwidth of the radar in the radio spectrum. The range is determined by a time delay and the phase velocity of the electromagnetic wave as:

$$r = c\tau/2, \quad (3)$$

where $c = 3 \times 10^8 \text{ ms}^{-1}$ and τ is the out and back time delay between the transmitter and the receiver. For resolution:

$$\Delta r = (c/2)\Delta\tau, \quad (4)$$

where $\Delta\tau$ is the resolution in time. This requires a bandwidth of Δf , where

$$\Delta f = c/(2 \Delta r). \quad (5)$$

Most HF ocean radars have bandwidths between 50 and 150 kHz, which correspond to a range resolution (pixel length) of 3 to 1 km, respectively. Long-range radars tend to have narrower bandwidths because of their lower operating frequency. The GBR radar has a bandwidth of 33 kHz, which corresponds to a range resolution of 4.5 km. As such, the smallest theoretical (Nyquist) tsunami wavelength that can be observed is 9 km, with the more realistic minimum being 13 to 18 km due to dispersion effects.

4.2 Time scales for radar observation

The time resolution for HF radars depends on the observation time required to make one surface current determination. For the GBR radar, the routine operation is to sample surface currents every 10 minutes, where each of the two stations operates for 5 minutes and then waits for 5 minutes. Some systems operate with surface currents produced routinely every 3 hours. To reduce the sampling time we have to trade off accuracy. For a phased array system such as the GBR radar, the trade-off is between time resolution and accuracy of the surface current values. Figure 5 shows the relationship where, at a radar operating frequency of 8 MHz (as in the case of the GBR radar), and a time-series length of 5 minutes, the surface current resolution is about 8 cm s^{-1} .

For direction finding radar systems, there is leakage from spectral resolution into the spatial domain. All the discussion here for the resolution of surface currents

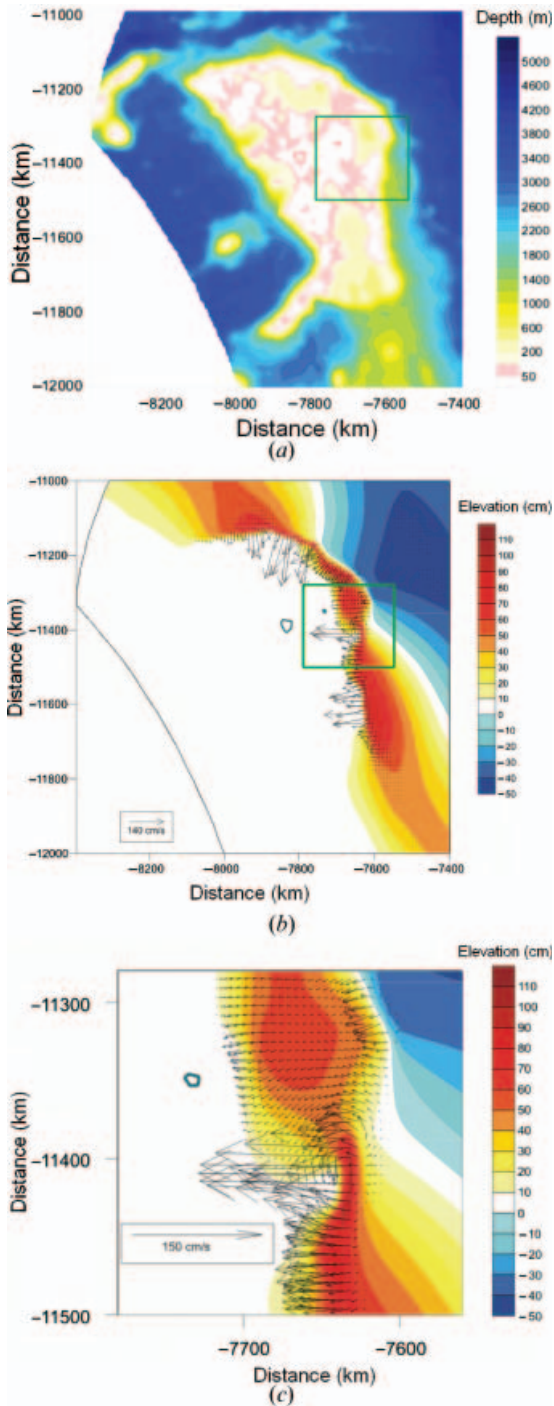


Figure 4. Model calculations for the impact of the 26 December 2004 tsunami on the Seychelles: (a) the bathymetry around the Seychelles shows a platform in otherwise deep water, (b) the large scale amplification of sea surface height (contours) and surface current (vectors) when the first tsunami wave encounters the edge of the continental shelf and (c) a section of the shelf-edge (corresponding to the box in (a) and (b)), which shows the area that could be monitored by a HF ocean radar.

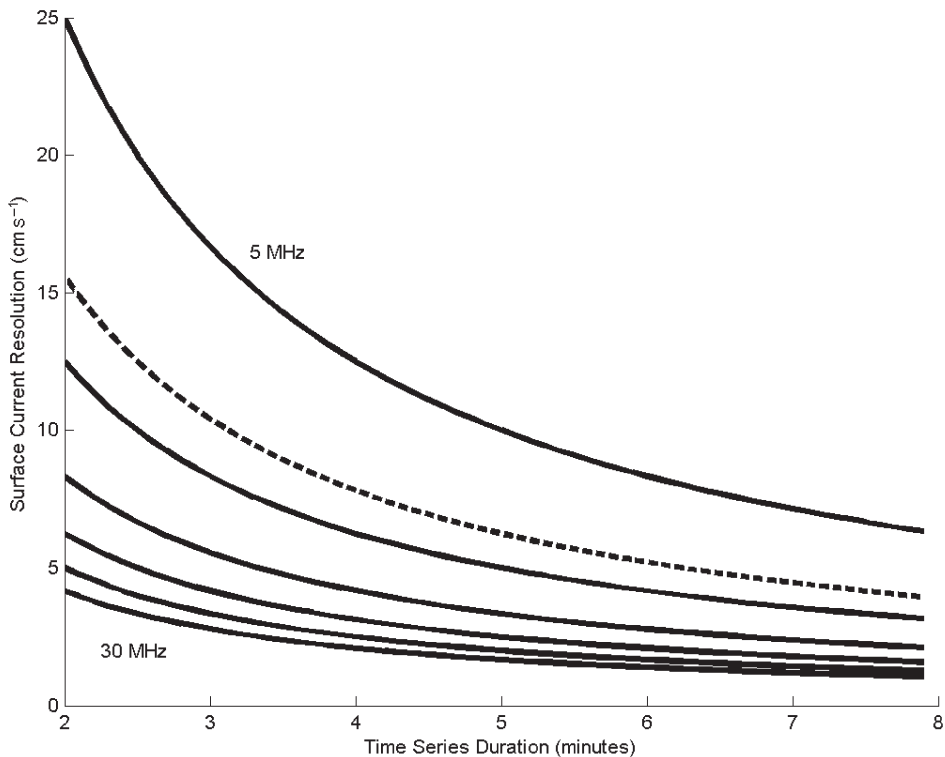


Figure 5. The resolution for surface current improves as the radar transmitter frequency increases. The parameter for the family of curves is radar frequency at values 5, 8 (dashed line), 10, 15, 20, 25 and 30 MHz. To achieve a resolution of 8 cm s^{-1} at an operating frequency of 8 MHz, one would need to integrate for a period of not less than 300 s. The GBR system operates at 8.348 MHz.

(including figure 5) applies to direction finding systems, but the length of the time series also impacts on spatial resolution (Barrick 1979).

4.3 Enhancement of tsunami detection by statistical pattern recognition

To some degree, there is an *a priori* pattern of large surface currents that occur when a tsunami encounters steep benthic gradients at the edge of a continental shelf. For each HF radar location it is possible to calculate a tsunami response pattern by numerical modelling methods, as illustrated in figure 4(c). To a first-order approximation (which needs to be confirmed) the response of the surface currents to the tsunami approaching the continental shelf, shown in figure 4(c), is independent of the direction of the source of the tsunami. This is because tsunami wave-fronts are refracted in deep water and will approach the shelf-edge within a small range of angles around orthogonal. This assumption can be tested for each site by numerical calculations provided by Greenslade *et al.* (2007). The surface current response therefore becomes a signature that we can look for in the data analysis process. Figure 4(c) shows the signature pattern of tsunami-driven currents at the Seychelles, and we can expect that other tsunamis generated in the Indian Ocean will have a similar spatial response there, but with different amplitudes.

Figure 6 shows an extraction of approximate radial surface currents that a HF radar on the main island of the Seychelles would observe. If we take a map of HF radar radial currents over that area at any other time, then the observed 2D scalar signal map, $\text{sig}(i,j)$, observed can be compared with the signature reference map, $\text{ref}(i,j)$, shown in figure 6, in a correlation analysis given by:

$$R = \frac{\sum \text{sig}(i,j) \text{ref}(i,j)}{\sqrt{\sum \text{sig}^2(i,j) \sum \text{ref}^2(i,j)}}, \tag{6}$$

where the summations are carried out over the whole 2D array of (i,j) .

A desk test was carried out by generating Gaussian noise across the ‘observed’ field of radial components of surface currents. We set the noise at the radar resolution limit of $\pm 13 \text{ cm s}^{-1}$ (estimated from figure 5 for an 8 MHz phased array radar taking independent time series every 300 s, and then allowing for equal fluctuations from all other noise sources) and introduced signal surface currents across the field at a range of fractions of the reference tsunami currents. Thus, the simulated observed data becomes:

$$\text{sig}(i,j) = \sqrt{2}\sigma \text{erfinv}(p) + f \text{ref}(i,j), \tag{7}$$

where p is a random number between -1 and 1 , f is the fraction of reference signal and σ is the standard deviation that we set at 13 cm s^{-1} . The function $\text{erfinv}(p)$ is the standard MATLAB inverse error function.

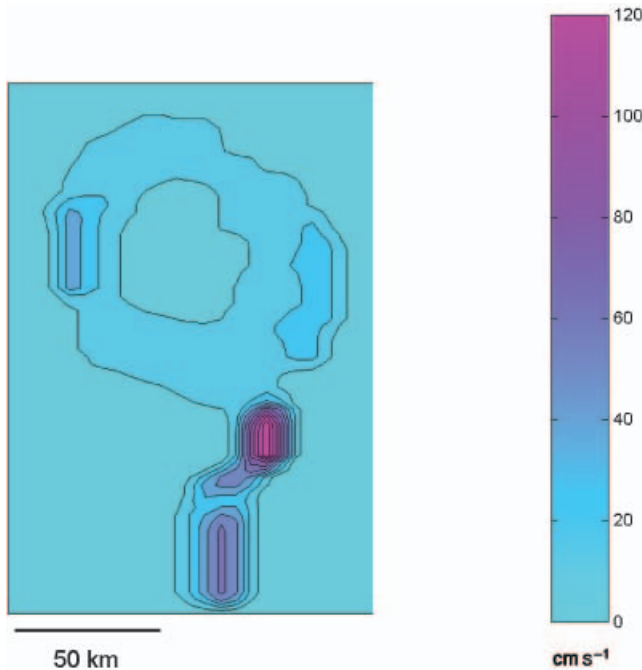


Figure 6. An extraction from figure 4(c) showing simulated contours of the radial currents that would be observed from a HF radar on the main Seychelles island. This is a spatial response from one tsunami wave crest that can be used as a mask for the detection of other tsunamis.

The results of the correlation analysis are shown in figure 7, where the abscissa is the fraction of signal combined with the noise, and the ordinate is the correlation coefficient calculated using equation (6). The uncertainty in the line is estimated by carrying out multiple runs of the simulation with the same fixed parameters and different sets of random noise; the dashed lines represent ± 2 standard deviations on the mean R value at each f . Figure 7 indicates that a correlation R value of 0.1 would be an acceptable detection limit for a tsunami event because it would have greater than 95% confidence of being greater than zero. The corresponding f value from figure 7 is about 8%, and certainly less than 10%.

It is clear therefore that an event should be detectable over the edge of the continental shelf for tsunamis as small as 1/10th of the size of the Boxing Day tsunami in the Indian Ocean, using an 8 MHz phased array radar that is repeatedly sampling time series every 300 s.

The calculations carried out here are for the first wave crest that approached the Seychelles Islands on 26 December 2004 and that were shown in figure 4. Subsequently, there were other troughs and crests that gave an oscillating amplified current at the edge of the shelf. The GBR phased array HF radar will resolve the oscillating currents in successive troughs and crests within the tsunami group. This time variation is useful to confirm the detection of a tsunami.

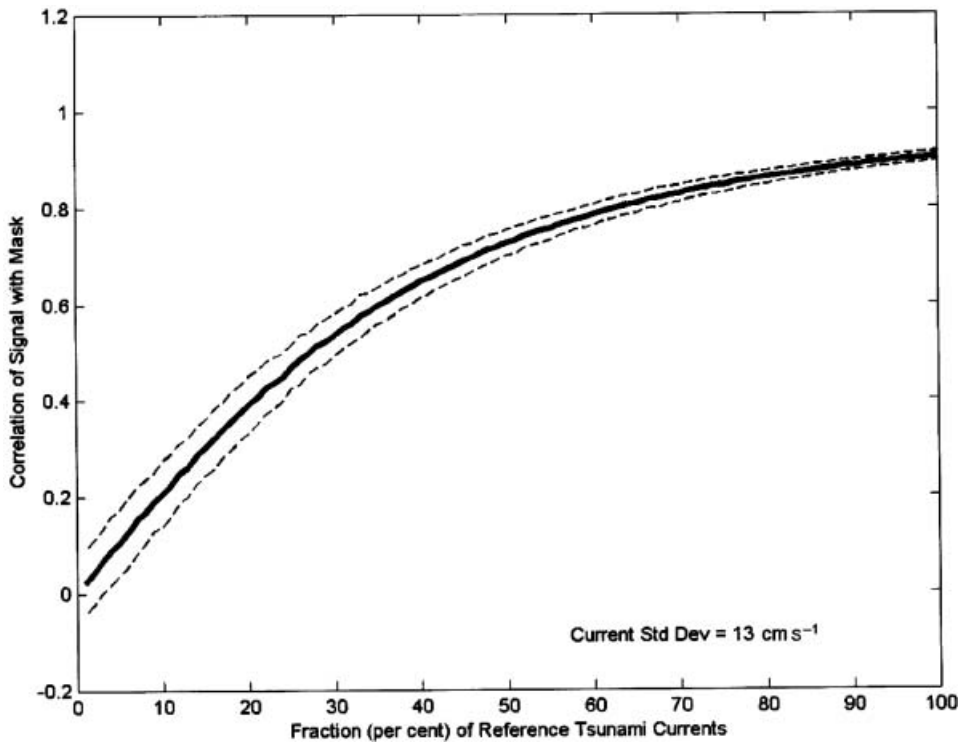


Figure 7. Correlation coefficient, $R(f)$ given in equation (6) as the fraction, f , of signal (from the template) increases and the fraction of noise ($1-f$) decreases. The solid line is a statistical mean, and the dashed lines show two standard deviations from the mean R .

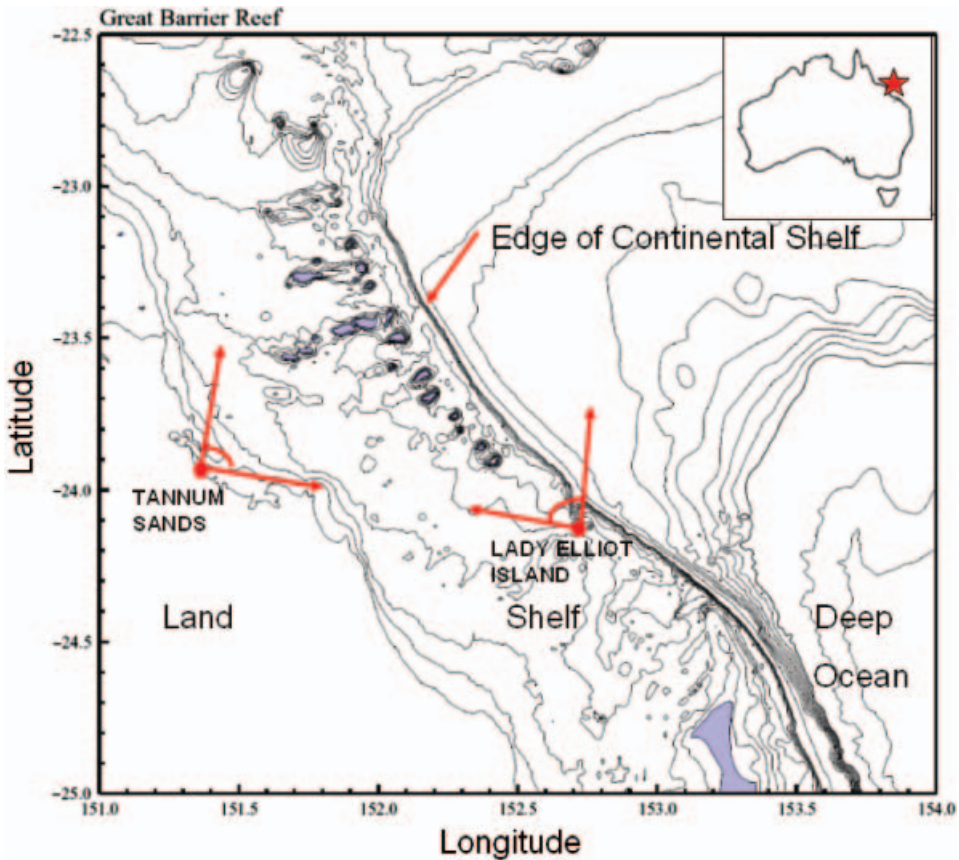


Figure 8. The western side of the map is mainland, and islands are shown lightly shaded. Bathymetry lines show a relatively flat shelf with depth around 40m and an abrupt bathymetric gradient about 100 km offshore just beyond the line of outer islands and reefs, giving way to a second, deeper, shelf and the deep ocean. The GBR HF radar has stations at 23°56.404' S, 151°22.193' E on the coast at Tannum Sands and at 24°6.792' S, 152°43.000' E on Lady Elliot Island, shown as solid dots on the diagram. The azimuthal scanning ranges of the beam of the phased array antennas are indicated by arrows. In a tsunami alert mode, the Lady Elliot Island station would be put on standby and the Tannum Sands station operated continuously.

4.4 A case study: the GBR phased array HF radar

The site layout for the GBR HF radar is shown in figure 8. The site is on the north east coast of Australia, at the southern end of the Great Barrier Reef. For routine surface current mapping, the stations are ideally situated so that they illuminate the study area of the Capricorn and Bunker Groups of islands and reefs approximately orthogonally. In a tsunami alert mode, we would put the Lady Elliot Island station on standby and operate the Tannum Sands station continuously, as the Tannum Sands radar scans nearly orthogonally to the shelf-break (see figure 8). Each individual measurement of radial surface current for the GBR radar, operating at 8 MHz and sampling time series for 150 s, is estimated to have a standard error of 13 cm s^{-1} (guided by figure 5). We have prior knowledge, modelled from the bathymetry, of the spatial variation of surface current velocities at the edge of the

continental shelf where the gradients in bathymetry are severe. This is illustrated in figure 4(c). For a typical radar configuration, we might expect the order of 100 spatial samples of radial current in a 6 km wide strip along the edge of the shelf that can be correlated with the template. By looking for a correlation R that is significantly greater than zero (at the two standard deviations level) between the observations and the template, we might expect to detect the presence of a tsunami that has surface current maxima of around 7.5 cm s^{-1} (from the calculation used for figure 7 with noise current set at 13 cm s^{-1}). This limit to the detection is about 1/20th of the currents modelled for the 26 December 2004 event at the Seychelles. Using a linear scaling assumption on the tsunami magnitudes to get orders of magnitude, this corresponds to detection of a tsunami that has water elevation of about 2.5 cm in the open ocean and which will have water elevation of the order of 13 cm at water depth of 10 m.

5. Conclusions

The 26 December 2004 tsunami depicted in figure 4 was a major event and of course the squirts of surface currents are very large – much greater than any tidal or wind-driven currents that we would normally expect to see at the shelf edge. The question that we address here is about the detection of small tsunamis, which, in terms of social and economic impact, might be negligible, but which would be most useful for studying tsunami properties and genesis.

The estimate that we make from this analysis approach is that the GBR HF radar operating at 8 MHz and taking successive time series every 150 s has the capability to detect tsunami events that are as little as 1/20th of the size of the Aceh tsunami on 26 December 2004. To achieve this, the HF radar would need to be switched to an alert mode of operation, presumably following a seismic alert. Its most effective use would be in assisting the warning network by filling the gap between deep-ocean sensors and coastal tide gauges and, in particular, in avoiding false alarms because of its high sensitivity compared with other sensors. Once validated, it could also possibly be used as a verification for tsunami models.

When the GBR radar is operating in its routine current mapping mode, each station records a 5 minute time series every 10 minutes. In this mode, the amplitude sensitivity is slightly improved, but the radar could then detect only tsunamis with wave period greater than 20 minutes. The most effective use in this mode is to generate an archive of data that can be trawled to find small and medium scale events to enable the study of the links between seismic activity and surface disturbances. It is a tool for studying tsunami genesis.

Acknowledgements

The HF radar deployed in the Great Barrier Reef region was funded under the Linkage Infrastructure Equipment and Facilities Grant LE0560892 from the Australian Research Council. Operational costs are being met by the Australian Coastal Ocean Radar Network, which is a part of the Australian Integrated Marine Observing System. The manuscript contents are solely the opinions of the authors and do not constitute a statement of policy, decision or position on behalf of NOAA or the US Government.

References

- BARRICK, D.E., 1979, A coastal radar system for tsunami warning. *Remote Sensing of the Environment*, **8**, pp. 353–358.

- BRYANT, E., 2001, *Tsunami: the Underrated Hazard* (Cambridge, UK: Cambridge University Press).
- GREENSLADE, D.J.M., SIMANJUNTAK, M.A., BURBIDGE, D. and CHITTLEBOROUGH, J., 2007, *A first-generation real-time tsunami forecasting system for the Australian Region*, BMRC report no 126, Bureau of Meteorology, Australia.
- GOWER, J., 2005, Jason 1 detects the 26 December 2004 tsunami. *American Geophysical Union EOS*, **86**, pp. 37–38.
- KINSMAN, B., 1965, *Wind Waves* (Englewood Cliffs, NJ: Prentice-Hall).
- SMITH, W.H.F., SCHARROO, R., TITOV, V.V., ARCAS, D. and ARBIC, B.K., 2005, Satellite altimeters measure tsunamis. *Oceanography*, **18**, pp. 11–13.